NASA Technical Memorandum 86434

NASA-TM-86434 19850023137

A NEW FINITE ELEMENT APPROACH FOR PREDICTION OF AEROTHERMAL LOADS - PROGRESS IN INVISCID FLOW COMPUTATIONS

KIM S. BEY, EARL A. THORNTON, PRAMOTE DECHAUMPHAI, R. RAMAKRISHNAN

JULY 1985

National Aeronautics and Space Administration

Langley Research Center
Hampton, Virginia 23665

A NEW FINITE ELEMENT APPROACH FOR PREDICTION OF AEROTHERMAL LOADS - PROGRESS IN INVISCID FLOW COMPUTATIONS

Kim S. Bey
NASA Langley Research Center
Hampton, Virginia

Earl A. Thornton, Pramote Dechaumphai, and R. Ramakrishnan
Old Dominion University
Norfolk, Virginia

Abstract

Recent progress in the development of finite element methodology for the prediction of aerothermal loads is described. Two dimensional, inviscid computations are presented, but emphasis is placed on development of an approach extendable to three dimensional viscous flows. Research progress is described for: (1) utilization of a commercially available program to construct flow solution domains and display computational results, (2) development of an explicit Taylor-Galerkin solution algorithm, (3) closed form evaluation of finite element matrices, (4) vector computer programming strategies, and (5) validation of solutions. Two test problems of interest to NASA Langley aerothermal research are studied. Comparisons of finite element solutions for Mach 6 flow with other solution methods and experimental data validate fundamental capabilities of the approach for analyzing high speed inviscid compressible flows.

Nomenclature

A	element area
D	solution domain
E_t	total energy
E,F	flux components in x and y directions
$\bar{E},\bar{F}$	artificial viscous flux components
$\|J\|$	determinant of Jacobian
L	length of element side
M	Mach number
$[M]$	mass matrix
$[N]$	element interpolation functions
$\hat{n}$	unit normal vector to surface
l,m	components of unit normal vector
p	pressure
r	number of nodes per element
S	solution domain boundary
s	surface coordinate
t	time
Δt	time step
u	scalar variable, eq. (4)
U	typical conservation variable
V	element volume
$\bar{V}$	velocity vector
u,v	velocity components in x and y directions
x,y,z	coordinate directions
γ	ratio of specific heats
ρ	density
ξ,η,ζ	element natural coordinates

Subscripts

D	constant element quantity, eq. (7)
i	index for node
s	constant surface quantity, eq. (10)
∞	free stream

Superscripts

e	element quantity
n	time step

Introduction

Thermal deformations and stresses induced by aerodynamic heating on high speed vehicles are an important concern in structural design. Aerodynamic heating may have a significant effect on the performance of the structure, and effective techniques for predicting the heating and the thermal-structural responses are required. Typical flight vehicles that have significant aerothermal-structural interactions are shown in figure 1 and include hypersonic cruise vehicles, the space shuttle, and advanced space transportation systems. Numerical methods such as finite difference methods and finite element methods play a significant role in fluid, thermal and structural analyses. Finite difference methods are the predominant numerical methods for computational fluid dynamics (CFD)[1]. A major problem in finite difference CFD is the generation of grids for realistic three dimensional vehicles such as finned projectiles or complete aircraft. The development of well-constructed CFD grids has been the subject of intensive research for several years. However, as noted in reference 2, the generation of a single grid that discretizes the entire flow region for a complex configuration is an extremely difficult and sometimes impossible task. These difficulties have led to recent research into alternative approaches for handling complex geometries including zonal schemes[2] and the finite volume approach[3].

Both finite differences and finite elements are used for thermal problems, but finite element methods are the predominant numerical methods for structural analysis[4]. Finite element methods are used extensively for structural analysis because of their capability to analyze a wide variety of realistic structures. The availability of general purpose finite element programs provide analysts a capability

to perform static and dynamic analyses with a spectrum of one, two, and three dimensional elements that can be used to represent accurately virtually any structure. The integration of these analysis programs with modern computer graphics capabilities provides the basis for computer aided design. For these reasons, finite element methods are also finding increasingly wider acceptance for structural heat transfer analysis particularly where a thermal-stress analysis is of interest.

Finite element methods are relatively immature for flow analysis in comparison to the finite difference method. Although finite elements have been applied to flow problems since about 1974, major emphasis has been placed on incompressible flows. Reference 4 describes finite element approaches used for incompressible flows and provides the principal references to finite element flow literature through 1982. A survey paper[5] summarizes progress of finite elements in fluid mechanics for the decade from 1974-1984. A 1982 assessment[6] of the finite element method's capability for the analysis of viscous compressible flows identifies early papers dealing in that area. Through 1982 only modest efforts had been made to develop finite elements for high speed compressible flows for either inviscid or viscous fluids. Researchers in the Aerothermal Loads Branch at NASA Langley decided that finite element methods offered potential for further development particularly for applications to complex aerospace vehicles with strong aerothermal-structural interactions. A research program with this goal was initiated in 1983. The principal motivations for investigation of finite elements for compressible flows are its inherent capability to handle complex geometries and the basic ability to analyze fluid, thermal, and structural interactions with a single methodology. The researchers believe that finite element methods may help alleviate some of the difficulties encountered by finite difference methods in flow problems, but recognize that much research remains to be done before finite element methodology becomes competitive with finite difference methods for predicting aerodynamic heating on high speed flight vehicles.

Research is underway at the NASA Langley Research Center to improve the capabilities and efficiency of finite element high speed compressible flow analysis methods and to develop more efficient integration of finite element fluid, thermal and structural analyses. The focus of the research is the prediction of aerothermal loads for complex three dimensional bodies. The research combines analyses with experimental studies conducted in the 8' High Temperature Tunnel (8' HTT) at NASA Langley[7]. The aerothermal loads research includes aerodynamic heating on control surfaces[8], pronounced localized heating effects on wavy surfaces[9] and in shuttle tile gaps[10].

Finite element methodology for compressible flow is under development by a team of University, industry, and NASA researchers. The purpose of this paper is to describe some of the recent progress in the development of the finite element compressible flow analysis methodology. The paper details progress in two dimensional inviscid flow computations with emphasis on the approaches being investigated to provide efficient model generation and computations for complex three dimensional flow domains. To develop the new approach, research is proceeding in five areas: (1) model generation and graphic displays, (2) algorithm development, (3) finite element matrices evaluations, (4) vector computer programming techniques, and (5) validation of the finite element approach. This paper highlights research in these areas.

Model Generation and Display Capability

The development of the model generation and display capability is based on currently available methodology for finite element modeling of geometries. Finite element modeling of geometrical shapes is well-developed in structural mechanics, and this technology can be exploited to model and represent graphically the continuum models for complex flows. The commercially available PATRAN-G (Trademark of PDA Engineering)* program[11] has been selected to generate flow models and display computational results. PATRAN offers mature state-of-the-art capability for geometrical modeling and results display for finite element analyses. Many of PATRAN's very general capabilities can be used advantageously for finite element flow analysis.

Modeling solution domains with PATRAN begins with creation of a geometric representation of the computational domain. A two dimensional computational domain is represented by a number of regions, called patches, whose edges are described by parametric cubic lines. For a three dimensional computational domain, surface patches are used to establish solid regions called hyperpatches. A finite element mesh can then be created by dividing patches or hyperpatches into a number of nodes and elements. Different element types, such as triangles and quadrilaterals for 2D meshes and tetrahedrons and hexahedrons for 3D meshes can be assigned to suit the analysis and finite element program requirements.

Examples of 2D and 3D computational domains are shown in figures 2 and 3. Figure 2a shows the patch representation of the flow field in a cove formed by a wing and elevon juncture. Figure 2b shows a very crude finite element mesh of the cove for illustrative purposes. Figure 3a shows a cutaway view of a hyperpatch representation of the computational domain for flow around a cylindrical protuberance. The hyperpatch representation is shown with hidden lines removed and drawn with dotted lines, high-

*Use of this commercial product does not imply endorsement by NASA.

lighting selected hyperpatches. Figure 3b shows a hidden-line view of the finite element mesh.

Translator and inverse translator programs have been developed to interface PATRAN with the flow analysis. The translator program[12] uses the output file generated by PATRAN to produce the complete input data file required for a flow analysis. In addition to the basic input data of nodal coordinates and element nodal connections, the translator generates the flow initial conditions, boundary conditions, and normal vectors along slip boundaries. This additional information is distinct from that required by finite element thermal-structural models currently supported by PATRAN. After the flow analysis is completed, the solution is translated into the format required by PATRAN for displaying computational results using the inverse translator program. Figure 4 shows schematically the computer usage for the flow analyses and the role of the translator and inverse translator programs.

Finite Element Solution Algorithm

Two general classes of explicit solution algorithms are being investigated: (1) Taylor-Galerkin algorithms, and (2) Petrov-Galerkin algorithms. The Taylor-Galerkin algorithm was first developed by Donea[13-14] and applied to compressible flows by Lohner, Morgan, and Zienkiewicz[15-16]. Petrov-Galerkin algorithms have been applied to compressible Euler equations by Hughes and Tezduyar[17-18]. A preliminary evaluation of these algorithms appears in reference 19. This paper utilizes the Taylor-Galerkin algorithm.

The basic concept of Taylor-Galerkin algorithms is to use: (1) Taylor series expansions in time to establish recurrence relations for time marching, and (2) the method of weighted residuals with Galerkin's criteria to develop the finite element matrix equations describing the spatial distribution of the flow variables. A variant of a two time level Taylor-Galerkin algorithm proposed by Morgan and Lohner is used in this paper.

The solution algorithm is applied to the basic flow equations in conservation form,

$$\frac{\partial\{U\}}{\partial t} + \frac{\partial\{E\}}{\partial x} + \frac{\partial\{F\}}{\partial y} = 0 \qquad (1)$$

where {U} is the vector of conservation variables, {E} and {F} are vectors of the flux components of mass, momentum and energy.

The vectors {U}, {E}, and {F}, are given by

$$\{U\}=\begin{Bmatrix}\rho\\ \rho u\\ \rho v\\ \rho E_t\end{Bmatrix},\quad \{E\}=\begin{Bmatrix}\rho u\\ \rho u^2+p\\ \rho uv\\ (\rho E_t+p)u\end{Bmatrix},\quad \{F\}=\begin{Bmatrix}\rho v\\ \rho vu\\ \rho v^2+p\\ (\rho E_t+p)v\end{Bmatrix} \qquad (2)$$

where ρ is density, u and v are the velocity components, and E_t is the total energy. The pressure p is given by the ideal gas law,

$$p = \rho\,(\gamma-1)\,[E_t-1/2\,(u^2+v^2)] \qquad (3)$$

Equation (1) is solved subject to appropriate initial and boundary conditions. Consider a solution domain D bounded by a surface S, (Fig. 5.). The initial conditions consist of specifying the distributions of the conservation variables at time zero. Typical boundary conditions include: (1) specifying all conservation variables for supersonic inflow on a segment of the boundary S_1, (2) requiring $\bar{V}\cdot\hat{n} = 0$ on a slip boundary S_2, where $\hat{n}$ is a unit vector normal to the surface and $\bar{V}$ is the velocity vector, and (3) using appropriate boundary conditions on the outflow surface S_3. For supersonic outflow surfaces, the conservation variables are unknown and completely defined by the upstream flow. This natural boundary condition consists of surface integrals of flux components to be derived in the finite element formulation. For subsonic outflow surfaces there is a downstream dependency that can be satisfied by specifying pressure at the outflow plane.

The solution domain D is divided into an arbitrary number of elements of r nodes each. Figure 5 shows typical quadrilateral elements (r=4) used in this paper. For simplicity, the finite element formulation will be given for a single scalar equation,

$$\frac{\partial u}{\partial t} + \frac{\partial E}{\partial x} + \frac{\partial F}{\partial y} = 0 \qquad (4)$$

where the variables u, E, and F are analogous to the corresponding vector quantities in eq. (1). Let $\{u\}^n$ denote the element nodal values of the flow variables $u(x,y,t)$ at time t_n. The time step Δt spans two typical times t_n and t_{n+1} in the transient response. The computation proceeds through two time levels, $t_{n+1/2}$ and t_{n+1}. At time level $t_{n+1/2}$, values for u that are constant within each element are computed explicitly. At time level t_{n+1}, the constant element values computed at the first time level are used to compute nodal values for u. In the time level t_{n+1} computations, element contributions are assembled to yield the global equations for nodal unknowns. The resulting equations are approximately diagonalized to yield an explicit algorithm.

Time Level $t_{n+1/2}$

To advance the solution to time level $t_{n+1/2}$, a truncated Taylor series yields

$$u(x,y,t_{n+1/2}) = u(x,y,t_n) + \frac{1}{2}\,\Delta t\frac{\partial u}{\partial t}(x,y,t_n) \qquad (5)$$

Then eq. (4) is introduced on the right hand side of eq. (5) so that

$$u(x,y,t_{n+1/2}) = u(x,y,t_n) - \frac{1}{2}\Delta t\left[\frac{\partial E}{\partial x}(x,y,t_n) + \frac{\partial F}{\partial y}(x,y,t_n)\right] \quad (6)$$

At time level $t_{n+1/2}$, the dependent variable $u(x,y,t_{n+1/2})$ is assumed to have a constant value $u_D^{n+1/2}$ within an element. Since the dependent variable has the constant value $u_D^{n+1/2}$ within an element, the flux components $E^{n+1/2}$ and $F^{n+1/2}$ are constant within an element as well.

At time level t_n in the response u, E, and F vary within an element and are interpolated from nodal values. Thus, the following spatial approximations are used within an element,

$$u^e(x,y,t_{n+1/2}) = u_D^{n+1/2} \quad (7a)$$

$$u^e(x,y,t_n) = [N(x,y)]\{u\}^n \quad (7b)$$

$$E^e(x,y,t_n) = [N(x,y)]\{E\}^n \quad (7c)$$

$$F^e(x,y,t_n) = [N(x,y)]\{F\}^n \quad (7d)$$

where $[N(x,y)]$ denotes element interpolation functions and $\{u\}^n$ is a vector of the element nodal quantities. For a typical quadrilateral element the interpolation functions are bilinear, and in a local natural coordinate system (see ref. 4) have the form

$$N_i = 1/4\ (1+\xi_i\xi)\ (1+\eta_i\eta) \qquad i=1,2,3,4 \quad (8)$$

where ξ_i and η_i denote the nodal coordinates $(\xi_i,\eta_i=\pm1)$ of the element in the ξ-η plane. The equations for $u_D^{n+1/2}$ for each element are derived by the method of weighted residuals. The spatial approximations given in eqs. (7) are introduced into eq. (6) to give a residual; the result is multiplied by a weighting function which in this case is unity. Finally, the weighted residual is integrated over the area A of the element. The result is,

$$A\,u_D^{n+1/2} = \int_A [N]\,dA\,\{u\}^n - \frac{\Delta t}{2}\int_A\left[\frac{\partial N}{\partial x}\right]dA\,\{E\}^n - \frac{\Delta t}{2}\int_A\left[\frac{\partial N}{\partial y}\right]dA\,\{F\}^n \quad (9)$$

With eq. (9), the dependent variable $u_D^{n+1/2}$ for each element can be computed explicitly using nodal values for u, E and F from the previous time t_n. The constant element variable $u_D^{n+1/2}$ may be interpreted as a weighted average of an element's nodal values at time t_n. A later section will discuss the evaluation of the three integrals that appear on the right hand side of eq. (9).

In advancing the solution to the next time level, the values of the dependent variables on the outflow surface will be required also. Let $u_s^{n+1/2}$ denote the surface value on a typical element edge IJ on the surface S_3 in figure 5. Following the approach used previously, $u_s^{n+1/2}$ is assumed constant on edge IJ at time $t_{n+1/2}$, but at time t_n u, E and F vary along the edge. Thus the following approximations are used on an element edge on S_3,

$$u^e(x,y,t_{n+1/2}) = u_s^{n+1/2} \quad (10a)$$

$$u^e(x,y,t_n) = [N(s)]\{u\}^n \quad (10b)$$

$$E^e(x,y,t_n) = [N(s)]\{E\}^n \quad (10c)$$

$$F^e(x,y,t_n) = [N(s)]\{F\}^n \quad (10d)$$

where $[N(s)]$ denotes the interpolation functions along an element edge. Using the method of weighted residuals, the values for $u_s^{n+1/2}$ are derived by integrating over the length L of an element edge. Hence

$$L\,u_s^{n+1/2} = \int_L [N]ds\,\{u\}^n - \frac{\Delta t}{2}\int_L\left[\frac{\partial N}{\partial x}\right]ds\,\{E\}^n - \frac{\Delta t}{2}\int_L\left[\frac{\partial N}{\partial y}\right]ds\,\{F\}^n \quad (11)$$

Thus, eqs. (9) and (11) can be used to advance explicity the element and surface values of the dependent variables to $t_{n+1/2}$. Beginning with nodal values of $\{u\}^n$, $\{E\}^n$, and $\{F\}^n$ at time t_n, eq. (9) is used to compute constant values $u_D^{n+1/2}$ for each element. In a similar way, eq. (11) is used to compute constant surface values $u_s^{n+1/2}$ for element edges on the outflow boundaries. These values are computed explicity by looping through all elements and element edges on outflow boundaries.

Time Level t_{n+1}

To advance the solution to t_{n+1}, forward and backward truncated Taylor series expansions at $t_{n+1/2}$ are used to write the approximation

$$u(x,y,t_{n+1}) = u(x,y,t_n) + \Delta t\,\frac{\partial u}{\partial t}(x,y,t_{n+1/2}) \quad (12)$$

Then following the approach used previously, eq. (4) is introduced on the right hand side to yield

$$u(x,y,t_{n+1}) = u(x,y,t_n) - \Delta t\left[\frac{\partial E}{\partial x}(x,y,t_{n+1/2}) + \frac{\partial F}{\partial y}(x,y,t_{n+1/2})\right] \quad (13)$$

At time levels t_n and t_{n+1} the variables u, E and F are interpolated within an element by eqs. (7b - 7d), respectively. The equations for the nodal values for $\{u\}^{n+1}$ can next be derived by the method of weighted residuals

using the interpolation functions $N_i(x,y)$ as weighting functions in the standard way.[4] In this process, the last term in eq. (13) is integrated by parts. These operations yield equations for the nodal values of a single element,

$$[M]\{u\}^{n+1} = [M]\{u\}^{n} + \Delta t \int_A \left|\frac{\partial N}{\partial x}\right| dA\, E(t_{n+1/2}) + \Delta t \int_A \left|\frac{\partial N}{\partial y}\right| dA\, F(t_{n+1/2}) + \{R\}^{n+1/2} \quad (14)$$

where

$$[M] = \int_A [N]^T [N]\, dA \quad (15)$$

and

$$\{R\}^{n+1/2} = -\Delta t \int_L \left[l\, E_s^{n+1/2} + m\, F_s^{n+1/2} \right] \{N\}\, ds \quad (16)$$

In eq. (16) l and m are the components of the unit normal vector $\hat{n}$. Following usual finite element procedures, the element matrices given in eqs. (14) and (16) can be assembled to form system (global) equations.

The matrix [M] defined by eq. (15) is customarily called the element consistent mass matrix. The term mass matrix is used because the matrix arises from the unsteady partial derivative $\partial u/\partial t$ which represents acceleration in structural dynamics. In structural dynamics, the coefficient matrix of the acceleration term actually has units of mass and is called the mass matrix. The term, consistent, is used to distinguish these matrices from diagonal mass matrices that arise from other discretization methods. A consistent mass matrix has off-diagonal terms that couple the element variables on the left hand side of eq. (14)resulting in an implicit scheme. In non-fluid applications, consistent mass matrices often result in improved time accuracy of solutions, although this observation has not been demonstrated conclusively for compressible fluids.

To yield an explicit algorithm the consistent mass matrix [M] has been diagonalized for the present computations. The diagonal elements are computed from[4]

$$M_i = \int_A N_i\, dA \qquad i = 1,2,\ldots,r \quad (17)$$

In the applications to be presented, the focus is on steady-state solutions so that time accuracy of the response computation is not an issue.

The last three terms on the right hand side of eq. (14) depend on element and surface values of the flux components evaluated at time level $t_{n+1/2}$. Note that the last term $\{R\}^{n+1/2}$, given by eq. (16), uses values of the fluxes E and F on the element edges lying on the outflow surface, S_3. The dependent variables $u_s^{n+1/2}$ given by eq. (11) are used to compute E_s^{n+1} and $F_s^{n+1/2}$. The vector $\{R\}^{n+1/2}$ represents the natural boundary condition for outflow surfaces mentioned previously. No other boundary condition is imposed on supersonic outflow surfaces.

The Taylor-Galerkin algorithm presented in the foregoing is based on the work of Lohner, Morgan, and Zienkiewicz[15-16]. The principal differences in the present form of the algorithm are the introduction of the surface quantities represented by eq. (11) and the use of quadrilateral elements. In reference 15 and 16, the boundary terms are treated differently and triangular elements are used. These references discuss similarities of the algorithm with second order finite difference methods such as Lax-Wendroff and a two step difference method by Burstein. The two time level Taylor-Galerkin algorithm is conditionally stable. For the diagonal mass matrix approach used herein the time step must satisfy the CFL criterion.

For problems with strong shocks artificial viscosity is used to reduce oscillations typical of second order accurate approximations. The form used in this formulation is due to Lapidus[20], and consists of introducing artificial viscous flux components $\bar{E}$ and $\bar{F}$ where

$$\bar{E} = \lambda A \left|\frac{\partial u}{\partial x}\right| \frac{\partial U}{\partial x} \quad (18a)$$

$$\bar{F} = \lambda A \left|\frac{\partial v}{\partial y}\right| \frac{\partial U}{\partial y} \quad (18b)$$

where λ is an adjustable constant, A is the element area, and U is a typical conservation variable. Computational experience has shown that $1<\lambda<2$ provides acceptable solution convergence without excessive smearing of shocks. In the computations, the nodal values $\{U\}^{n+1}$ at time level t_{n+1} are corrected (or smoothed) by incremental values $\{\Delta U\}$ computed from

$$[M]\{\Delta U\} = \{R\} \quad (19a)$$

where

$$\{R\} = \Delta t \int_A \left[\bar{E}^{n+1} \left|\frac{\partial N}{\partial x}\right| + \bar{F}^{n+1} \left|\frac{\partial N}{\partial y}\right| \right] dA \quad (19b)$$

where $\bar{E}^{n+1}$ and $\bar{F}^{n+1}$ are the artificial viscous flux components evaluated at time level t_{n+1}. The element integrals in eq. (19b) are evaluated using four point Gauss quadrature.

Explicit Evaluation of Element Integrals

Element integrals for the Taylor-Galerkin algorithm shown in eqs. (9), (11), and (14-16) were evaluated in closed form to avoid expensive numerical integrations that are customary for quadrilateral elements. For two dimensional problems, these element integrals are either in the form of integration over the element area or along the element edge. As an example, the element mass matrix for a quadrilateral element, eq. (15), is given by

$$[M] = \int_{-1}^{1}\int_{-1}^{1} [N]^T[N] \left|J\right| d\xi\, d\eta \quad (20)$$

where $[N]^T$ is the vector of the element interpolation functions in terms of the element natural coordinates ξ and η. The determinant of the Jacobian $|J|$ that appears in the above equation represents the transformation from the element global coordinates x-y to natural coordinates ξ-η. The transformation permits the element integration to be evaluated over a square. The determinant of the Jacobian is given by[2]

$$|J| = \begin{vmatrix} \frac{\partial x}{\partial \xi} & \frac{\partial y}{\partial \xi} \\ \frac{\partial x}{\partial \eta} & \frac{\partial y}{\partial \eta} \end{vmatrix} \qquad (21)$$

For a typical 4-node quadrilateral element shown in figure 5, the determinant of the Jacobian is

$$|J| = \begin{vmatrix} \frac{\partial}{\partial \xi} \sum_{i=1}^{4} N_i x_i & \frac{\partial}{\partial \xi} \sum_{i=1}^{4} N_i y_i \\ \frac{\partial}{\partial \eta} \sum_{i=1}^{4} N_i x_i & \frac{\partial}{\partial \eta} \sum_{i=1}^{4} N_i y_i \end{vmatrix} \qquad (22)$$

The difficulty in evaluating the mass matrix in closed form arises because the integrand involves the determinant of the Jacobian above, which if completely expanded produces an algebraic expression with 128 terms. However, by realizing that because of the form of the interpolation functions the determinant of the Jacobian varies with the natural coordinates ξ and η in the form of second order polynomials, the mass matrix can be evaluated effectively by writing the determinant of the Jacobian in the form

$$|J| = \sum N_i |J|_i \qquad (23)$$

Where $|J|_i$ represents the value of the determinant of the Jacobian at the i^{th} node. Using eq. (8), the equations of $|J|_i$ can be evaluated directly. For example, for a typical element node I (Fig. 5),

$$|J|_I = |J(\xi=-1,\eta=-1)| = [(x_J-x_I)(y_L-y_I)-(x_L-x_I)(y_J-y_I)]/4 \qquad (24)$$

Using the determinant of the Jacobian in the form of eq. (23), the mass matrix shown in eq. (20) can be evaluated in closed form.

The approach described above can be extended directly for the evaluation of three dimensional hexahedral element integrals. Typical element integrals derived using the Taylor-Galerkin algorithm are in the same form as obtained for the quadrilateral element where the element integrations are either performed over the element volume or the element surface areas. As an example, the mass matrix for a hexahedral element is given by

$$[M] = \int_V [N]^T[N]\, dV = \int_{-1}^{1}\int_{-1}^{1}\int_{-1}^{1} [N]^T [N] |J|\, d\xi\, d\eta\, d\zeta \qquad (25)$$

where ξ,η,ζ are the element natural coordinates. The determinant of the Jacobian above, if completely expanded, contains approximately 200,000 terms. To evaluate the integral in closed form, the determinant of the Jacobian was written in the form of eq. (23). Lagrange polynomials for a 27-node hexahedral element are used because they contain complete polynomials of ξ,η,ζ as they appear in the determinant of the Jacobian.

The CPU time used by the closed form solution of the mass matrix has been investigated and compared with CPU times required for different orders of Gauss numerical integration for quadrilateral and hexahedral elements. Although CPU time savings for quadrilateral elements are large (a factor of 50 for all integrals), the CPU time savings for hexahedral elements is even more significant. Typical CPU times for evaluation of a hexahedral element mass matrix are compared in figure 6. The figure shows that the closed form solution reduces CPU time for an element mass matrix significantly. Time savings in excess of an order of magnitude are obtained from the closed form solution in comparison with the popular 8 point Gauss integration method. Computational savings from explicit evaluation of other hexahedral element matrices are shown in figure 7.

The time savings gained by explicit evaluation of the finite element integrals is an important step toward developing efficient finite element computations for large scale three-dimensional flow computations.

Vector Programming Strategies

The algorithms under evaluation are being implemented with vectorization strategies specifically for the Langley VPS 32 (a Cyber 205 with 16 million words of central memory). This computer achieves high computational speed when performing operations on long vectors. Vector lengths of at least 60 are required to justify vectorization efforts with maximum payoff achieved for vector lengths of 1000 or more. The predominant vector lengths in the vectorization scheme presented here are the number of elements in the finite element model with occasional operations using vector lengths equal to the number of nodes.

The critical vectorization tasks are for those operations that are repetitive and performed at every time step. For finite element algorithms, these operations are: (1) assembly of element contributions from the right hand side of eq. (14) into the global system of equations, (2) solution of the global system of equations, and (3) application of boundary conditions.

The assembly of element contributions into the global system of equations is the process in finite elements which differs most from other numerical techniques and requires special routines for vectorization. Nodal unknowns are stored in one dimensional arrays from 1 to the number of nodes in the model, and in general, node numbering may be arbitrary throughout the mesh. Assembly of element contributions is performed using the VPS 32 FORTRAN-supplied scatter routine which places an element contribution into the proper location in the system of equations based on the element connectivity (node numbers of I,J,K,L in figure 5). Every element that contains a particular node in its connectivity provides its own contribution to the system equations, therefore the assembly is an additive operation. "Scattering" alone would merely overwrite a previous element contribution. The special vector routine, then does an "additive scatter."

For an explicit scheme, solutions are obtained directly, so that operation (2) vectorizes naturally. Operation (3), the application of boundary conditions (fixed and slip) is an intrinsically scalar operation and difficult to vectorize. However, use of bit vectors to flag boundary nodes and use of VPS 32 FORTRAN supplied routines enables full vectorization of this operation.

The program flowchart for the Taylor-Galerkin algorithm is shown in fig. 8. Using closed form integration and explicit vectorization, the program averages computational speeds of 4×10^{-5} CPU sec/time step/node. The computational savings derived from explicit vectorization of the boundary condition subroutine is illustrated in Table I.

Table I. - Computational Savings by Vectorization of Boundary Condition Routine

	UNVECTORIZED (SECS)	VECTORIZED (SECS)
CPU TIME PER CALL	0.0066	0.00058
TOTAL CPU TIME 1200 CALLS	8.0	0.7
TOTAL PROGRAM CPU TIME	36.0	28.8
PERCENT OF CPU TIME SPENT	22.0%	2.0%

Validation of Finite Element Approach

To validate the finite element approach described in the previous section, two test problems are presented. These test problems are chosen for their relevance to the prediction of aerodynamic heating and because of the availability of comparison solutions or experimental data.

Panel Holder Leading Edge

The first problem is Mach 6.57 flow over the blunt leading edge of the panel holder[22], figure 9, used in the 8' HTT for testing a variety of configurations. The finite element model for the blunt leading edge of the panel holder at a 5° angle of attack, shown in figure 10, consists of 3200 quadrilateral elements and 3321 nodes. With the initial conditions of uniform Mach 6.57 flow and a maximum allowable time step of 0.5×10^{-7} seconds, a steady state solution was obtained in 3250 time steps. Convergence is considered achieved when the L_2 norm of the change in density decreases 3 orders of magnitude.

The density contours in figure 11 show the bow shock which forms ahead of the body and the expansion of the flow around the nose. Slight oscillations occur in the solution near the shock which is captured over 8 elements.

For comparison, solutions were also obtained from two other numerical techniques. A method of lines[23] shock fitting solution was obtained for a cruder mesh containing one-seventh the number of nodes. An upwinded finite volume[24] shock capturing solution was obtained for a mesh similar to the finite element mesh. Comparison of these solutions with the finite element solution is shown in figures 12 and 13. A comparison of the velocity distributions along the mesh exit is shown in figure 12. The shock fitting technique adjusts the mesh boundary to coincide with the shock so that the solution is obtained only up to the shock, while the shock capturing solutions extend through the shock into the freestream region. All three solutions agree well. The oscillations in the finite element solution in the freestream region do not appear in the finite volume solution because it uses a more sophisticated smoothing technique. Also, no attempt was made to fine tune the finite element solution by increasing the artificial viscosity. Figure 13 shows the distributions of Mach number and pressure on the body. The finite element solution for Mach number falls between the shock fitting and finite volume solutions. Both the finite element and finite volume techniques predict a lower Mach number after the expansion point than the shock fitting solution. The pressure distributions are virtually identical for all three techniques.

Wing-Elevon Cove

The configuration for a wing-elevon cove is depicted in figure 14 which shows a sketch of the Space Shuttle Orbiter and a simplified cross-sectional view of its structure at the juncture between the wing and elevon. Without the spring-loaded rub seal, the pressure differential across the windward and leeward surfaces of the wing would drive a portion of the hot boundary-layer flow into the cove where it would contact the aluminum load-bearing structure. To provide insight into the problem and provide a data base for future vehicle design, a full-

scale model of the wing-elevon cove was tested in the 8' HTT.[25] Supporting analytical studies were also undertaken using the 2D compressible Navier-Stokes equations[8], but only qualitative results were obtained. A partial cross section of the experimental model and instrumentation is shown in figure 15. The experimental parameters were the freestream conditions, the elevon deflection angle, and the cove leak area. For the finite element analysis a laminar flow case, test 11, in reference 25 was chosen. The test parameters for this case are the freestream conditions shown in figure 15, an elevon deflection angle of 25°, and a cove leak area equal to half the cove inlet area. The portion of the external hypersonic flow region used for the analysis is also shown in figure 15.

The finite element model of the cove, shown in figure 16, consists of 1665 quadrilateral elements and 1802 nodes. The specified inflow conditions and the fixed cove exit pressure were calculated from experimental data from instrumentation on the wing just ahead of the cove and just after the leak (figure 15). The initial conditions in the hypersonic region were the inflow conditions and in the cove were calculated from experimental data at the cove inlet. The converged solution required 40,000 time steps of 0.15E-6 seconds for a total CPU time of 3000 seconds on the VPS 32. A large number of time steps were required because the subsonic flow in the cove requires considerably more time to converge than the external supersonic flow.

The finite element solution is shown in figures 17 and 18. The Mach number contours (figure 17) show oscillations in the solution ahead of the shock and in the expansion region at the cove inlet. The solution shows the expansion of the flow around the wing trailing edge. A portion of the external flow enters the cove and flows subsonically ($M \leq 0.4$) through the leaking seal. The bulk of the external flow impinges on the elevon forming an oblique shock. The pressure contours (figure 18) are relatively smooth and clearly define the oblique shock which was captured over 8 elements. Figure 19 compares the finite element solution for pressure along the inner cove wall and elevon with experimental data. The experimental data shows that the pressure is nearly constant in the cove and rises gradually along the elevon. The finite element solution predicts the constant cove pressure with a steep pressure rise along the elevon. Figure 19 also shows the pressure on the elevon as approximated by oblique shock theory for a wedge angle of 25°. Downstream of the computational domain, the experimental data appears to be asymptotically approaching the oblique shock theory pressure. The finite element solution slightly overestimates the oblique shock theory pressure. The actual flow phenomena is complicated at the cove entrance by viscous effects not included in the present analysis. Viscous effects may account for the disagreement in the pressure predicted by the inviscid finite element analysis and the experimental data along the elevon (s>7).

Concluding Remarks

Recent progress in the development of finite element compressible flow methodology is described. The goal of the research is to provide an effective computational procedure for complex flight vehicles with significant aerothermal-structural interactions. Two dimensional inviscid flow computations are emphasized, and the approaches being investigated to provide efficient mesh generation and effective computations extendable to three dimensional flows are described. The mesh generation approach is based on currently existing finite element methodology used in structural mechanics. The commerically available PATRAN-G program is used, and many of PATRAN's very general capabilities for constructing representations of solution domains can be used advantageously for finite element flow analysis. To interface PATRAN with the flow analysis programs, interface programs have been developed.

A two-step, explicit Taylor-Galerkin solution algorithm is described. The algorithm is similar to earlier second order finite difference schemes and uses artificial viscosity to smooth oscillations in the vicinity of shocks. The element integrals that appear in the Taylor-Galerkin algorithm are evaluated in closed form for two dimensional quadrilateral and three dimensional hexahedral elements. Numerical calcuations show that CPU times can be reduced significantly by the closed form evaluation of the matrices. The algorithm has been implemented on the Langley VPS 32 vector computer with special programming strategies to insure computations with long vectors. Typical vector lengths equal the number of nodes or elements are employed.

To validate the approach, two test problems of interest to aerothermal research at NASA Langley were studied. The first problem is Mach 6.57 flow over the leading edge of a panel holder used in the NASA Langley 8' High Temperature Tunnel (8' HTT). The finite element solution is compared with a method of lines shock fitting solution and an upwinded finite volume shock capturing solution. The finite element solution smears the shock over about 8 elements and shows slight oscillations. The solutions generally show good agreement for Mach number and pressure on the body surface and velocity components on the outflow plane.

The second test problem considers a leaking space shuttle wing elevon cove. The effects of a leaking wing elevon seal have been studied previously in the 8' HTT using a full scale model. The complex cove geometry combined with Mach 6 external flow and subsonic cove flow have taxed previous computational approaches to the problem. The finite element solution modeled the complete, highly irregular cove geometry and captured essential features of the flow. The external shock on the wing was captured and the low Mach number subsonic flow in the cove was represented qualitatively. Comparison of the finite element predicted pressure distribution along the cove inner wall shows excellent agreement with experimental data within the cove, but the finite element solution overestimates the pressures on the elevon surface in the

supersonic outer flow. A possible source of this discrepancy is viscous flow effects at the cove entrance that are not included in the inviscid finite element analysis.

The two test problems have validated fundamental capabilities of the finite element approach for analyzing high speed inviscid compressible flows. The ground work has been established for further investigation of the approach for three dimensional flows and the extension to include viscous effects. Much research remains to be done to establish a robust, generally effective method for complex flight vehicles with strong aerothermal-structural interactions, but progress towards achieving this goal has been demonstrated.

References

[1]Anderson, D.A., Tannehill, J.C. and Pletcher, R.H., Computational Fluid Mechanics and Heat Transfer, Hemisphere Publishing Corporation, New York, 1984.

[2]Rai, Man Mohan; "An Implicit, Conservative, Zonal-Boundary Scheme for Euler Equation Calcuations," AIAA-85-0488, AIAA 23rd Aerospace Science Meeting, Reno, NV, Jan. 14-17, 1985.

[3]Jameson, Anthony and Baker, Timothy: "Solution of Euler Equations for Complex Configurations," AIAA-83-1929, AIAA 6th Computational Fluid Dynamics Conference, Danvers, MA, July 13-15, 1983.

[4]Huebner, K.H. and Thornton, E.A., The Finite Element Method for Engineers, Second Edition, John Wiley, New York, 1982.

[5]Zienkiewicz, O. C. in collaboration with Lohner, R.; Morgan, K.; Nakazawa, S: "Finite Elements in Fluid Mechanics - A Decade of Progress," Chapter to appear in Finite Elements in Fluids, Vol. 5, J. Wiley and Sons.

[6]Morgan, K. and Thornton, Earl A.: "Finite Element Analysis of Aerodynamic Heating in Three-Dimensional Viscous High Speed Compressible Flow: An Assessment," Department of Mechanical Engineering and Mechanics, Old Dominion University, Norfolk, VA, August 1982.

[7]Couch, Lana M. and Wieting, Allan R.: "Capability for Aerothermal-Structural Tests of Large-to-Full-Scale Components of Future Space Transportation Systems," AIAA Conference on Advanced Technology for Future Space Systems, Hampton, VA, May 1979.

[8]Wieting, A. R.; Walsh, J. L.; and Bey, K. S., "Aerothermal Environment in Control Surface Gaps in Hypersonic Flow - An Overview," AIAA-83-1483, AIAA 18th Thermophysics Conference, Montreal, Canada, June 1-3, 1983.

[9]Olsen, George C. and Smith, R. E.: "Aerothermal Loads Analysis for High Speed Flow over a Quilted Surface Configuration," AIAA-84-1630, AIAA 17th Fluid Dynamics, Plasma Dynamics and Lasers Conference, June 1984.

[10]Avery, Don E; Kerr, Patricia A; Wieting, Allan, R.: "Experimental Aerodynamic Heating to Simulated Shuttle Tiles," NASA TM-84654, April 1983.

[11]PATRAN-G Users Guide, PDA Engineering, Santa Ana, CA 92705.

[12]Dechaumphai, P. and Thornton, E.A., "Development of a Translator for Finite Element Computational Fluid Dynamics," Proceedings of the 2nd PATRAN Users Conference, H.H. Fong (editor), PDA Engineering, 1984.

[13]Donea, J., "A Taylor-Galerkin Method for Convective Transport Problems," Numerical Methods in Thermal Problems, edited by R.W. Lewis, J.A. Johnson and W. R. Smith, Proceedings of Third International Conference, Seattle, WA, August 2-5, 1983, Pineridge Press, Swansea, U.K.

[14]Donea, J., "Taylor-Galerkin Method for Convective Transport Problems," Int. J. Num. Meth. Eng., Vol. 20 (1984) pp. 101-120.

[15]Lohner, R., Morgan, K. and Zienkiewicz, O.C., "The Solution of Non-Linear Hyperbolic Equation Systems by the Finite Element Method," Int. J. Num. Meth. Fluids Vol. 4 (1984), pp. 1043-1063.

[16]Lohner, R., Morgan, K. and Zienkiewicz, O.C., "The Use of Domain Splitting With an Explicit Hyperbolic Solver," Comp. Meth. Appl. Mech. Engng. Vol. 45, (1984) pp. 313-329.

[17]Hughes, T.J.R., and Tezduyar, T.E., "Finite Element Methods for First Order Hyperbolic Systems with Particular Emphasis on the Compressible Euler Equations," NASA Ames NCA2-OR745-104, Oct. 1983.

[18]Tezduyar, T.E., and Hughes, T.J.R., "Finite Element Formulations for Convection Dominated Flows with Particular Emphasis on the Compressible Euler Equations," AIAA 21st Aerospace Sciences Meeting, Reno, NV, Jan. 10-13, 1983, AIAA Paper No.-83-0125.

[19]Thornton, E.A. and Ramakrishnan, R., "One Dimensional Time-Dependent Compressible Flow Solutions," Proceedings of Fifth International Symposium on Finite Elements and Flow Problems, G.H. Carey and J.T. Oden (editors), Texas Institute for Computational Mechanics, The University of Texas at Austin, 1984, pp. 407-411.

[20]Lapidus, A., "A Detached Shock Calculation by Second-Order Finite Differences," J. Comp. Phys. Vol. 2 (1967), pp. 154-177

[21]MACSYMA Reference Manual, The Mathlab Group, Laboratory for Computer Science, MIT, Cambridge, MA, December 1977.

[22]Deveikis, William, D. and Hunt, L. Roane: "Loading and Heating of a Large Flat Plate at Mach 7 in the Langley 8-Foot High Temperature Structures Tunnel," NASA TM D-7275, 1973.

[23]Hamilton III, Harris H., "Solution of Axisymmetric and Two-Dimensional Inviscid Flow Over Blunt Bodies by the Method of Lines," NASA TP 1154, April 1978.

[24]Walters, R. W. and Dwoyer, D. L., "An Efficient Iteration Strategy Based on Upwind/Relaxation Schemes for the Euler Equations," AIAA-85-1529-CP, to be presented at AIAA 7th CFD Conference, Cincinnati, OH, July 15-17, 1985.

[25]Deveikis, W. D., "Effects of Flow Separation and Cove Leakage on Pressure and Heat-Transfer Distributions Along a Wing-Cove-Elevon Configuration at Mach 6.9," NASA TP 2127, July 1983.

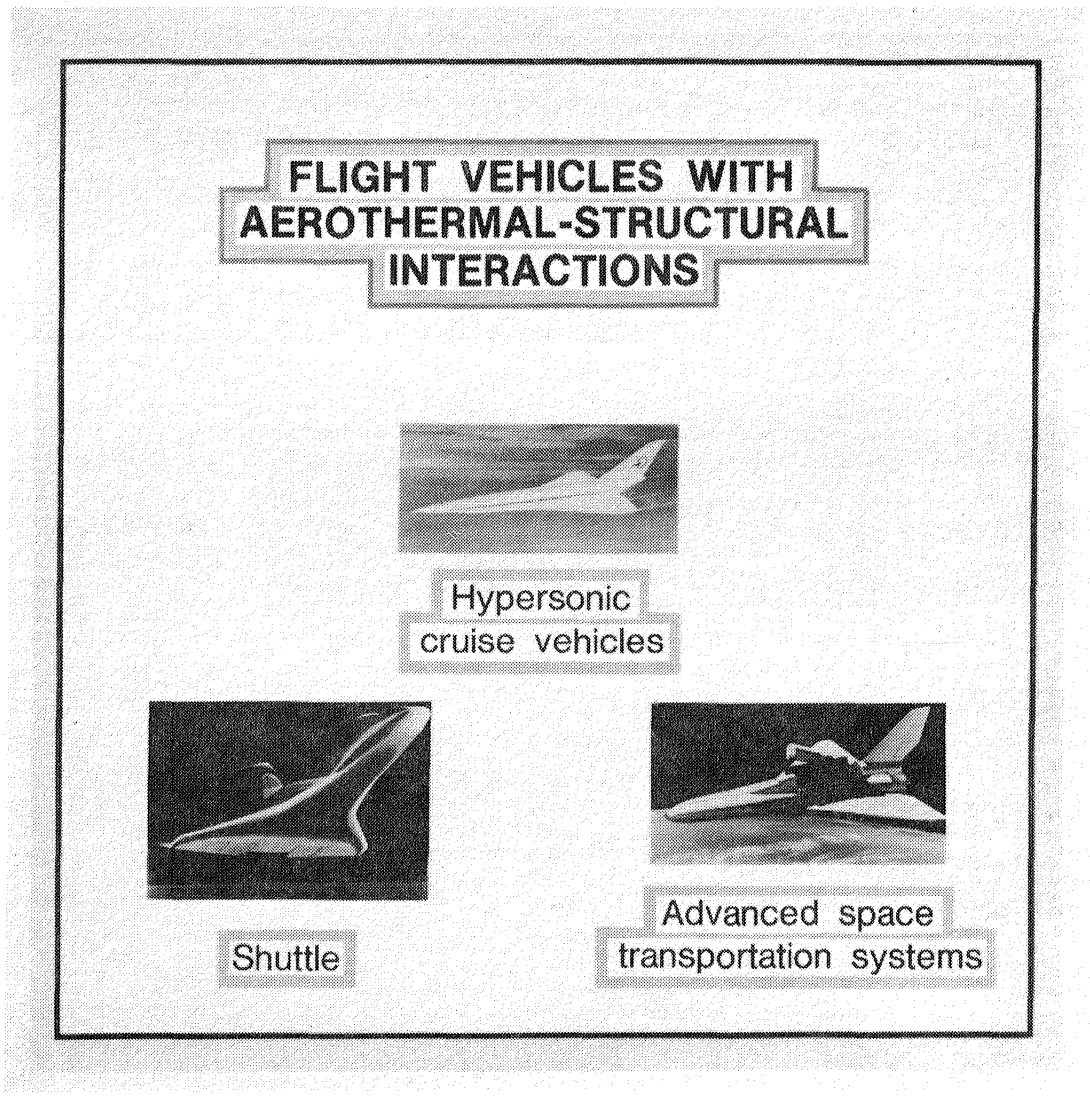

Fig. 1 Flight vehicles with aerothermal-structural interactions.

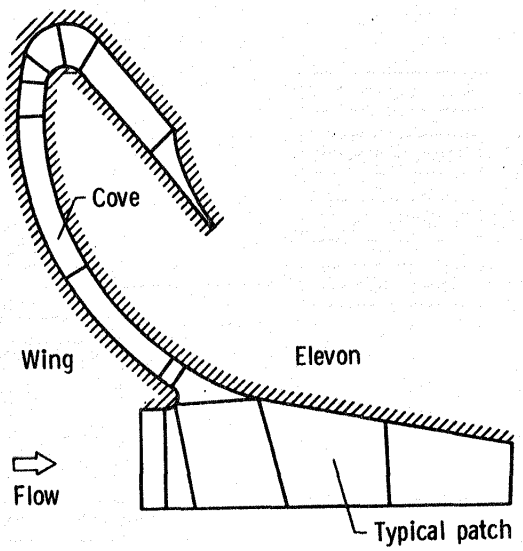

a) Patch representation of computational domain

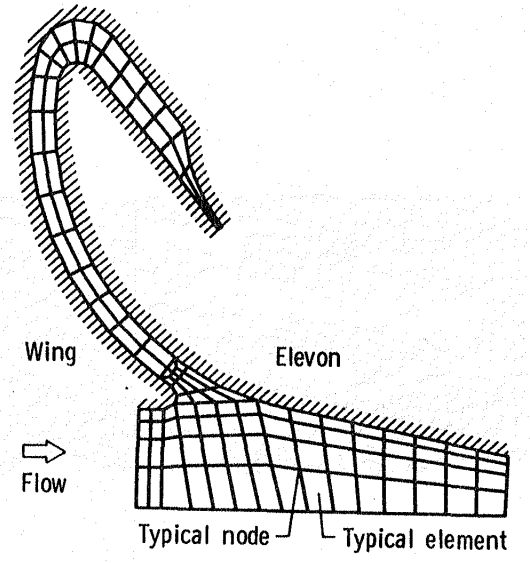

b) Crude finite element mesh

Fig. 2 Computational domain for flow in a wing-elevon cove.

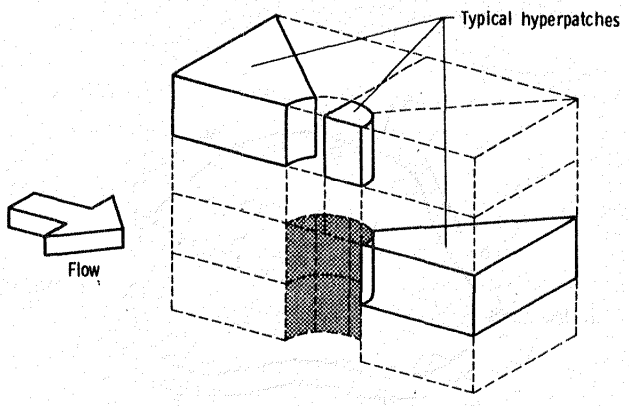

a) Hyperpatch representation of computational domain

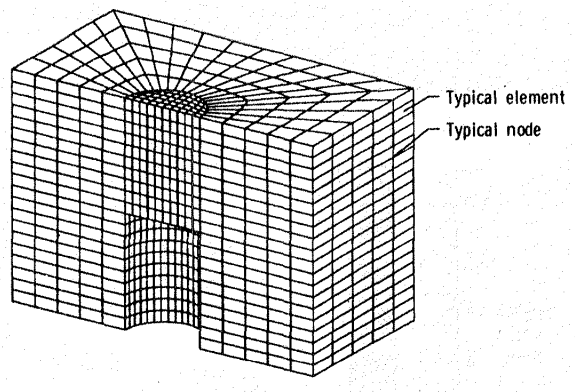

b) Finite element mesh

Fig. 3 Computational domain for flow past a cylindrical protuberance.

COMPUTER USAGE FOR FLOW ANALYSIS

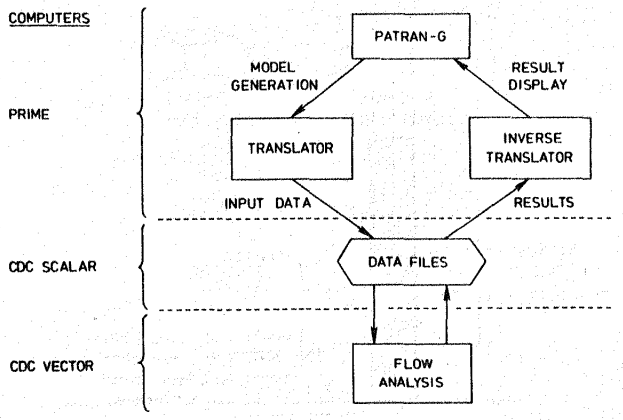

Fig. 4 Computer usage for flow analysis.

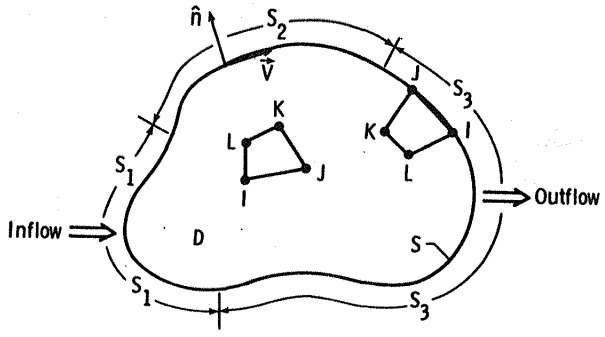

Fig. 5 Two dimensional finite element computational domain.

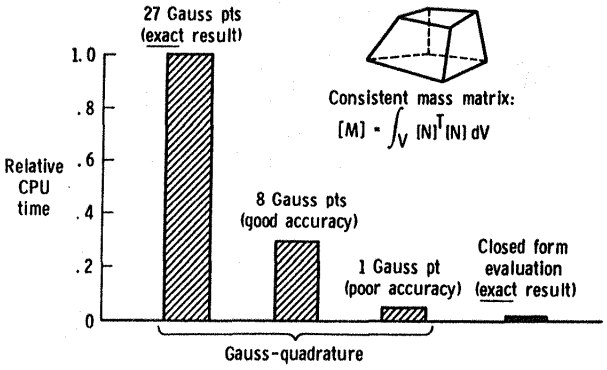

Fig. 6 Comparison of execution times for evaluation of hexahedral element mass matrix.

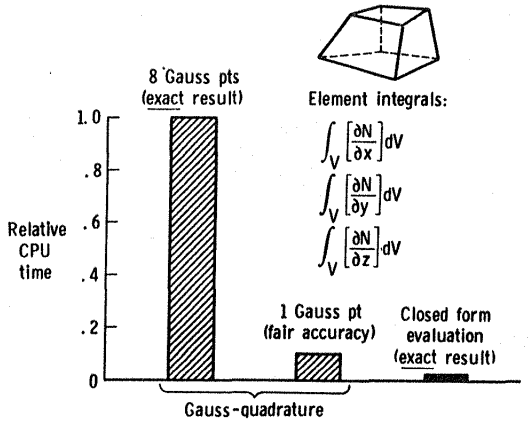

Fig. 7 Comparison of execution times for evaluation of hexahedral element matrices.

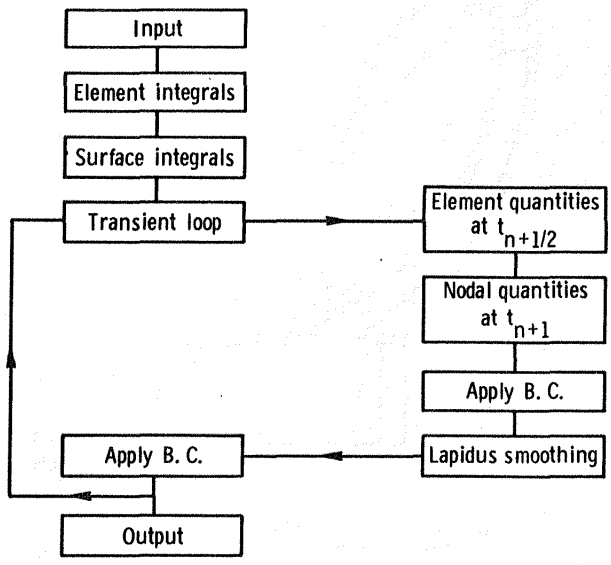

Fig. 8 Program flowchart for Taylor-Galerkin algorithm.

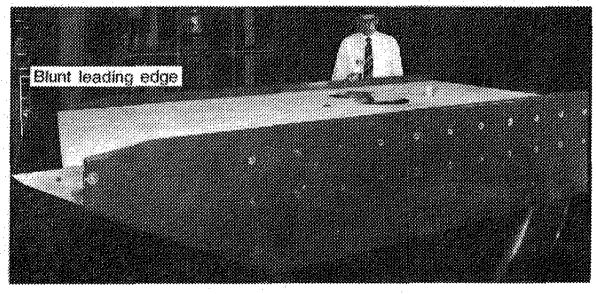

Fig. 9 Panel holder in 8-Foot High Temperature Tunnel (8' HTT).

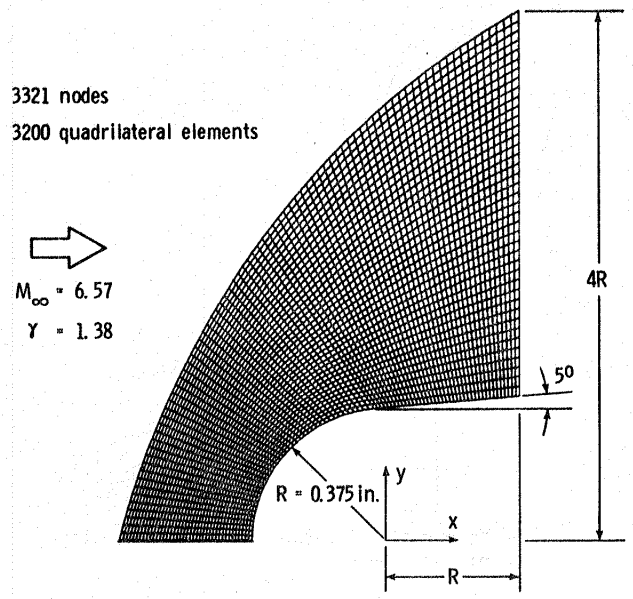

Fig. 10 Finite element mesh for blunt leading edge of 8' HTT panel holder.

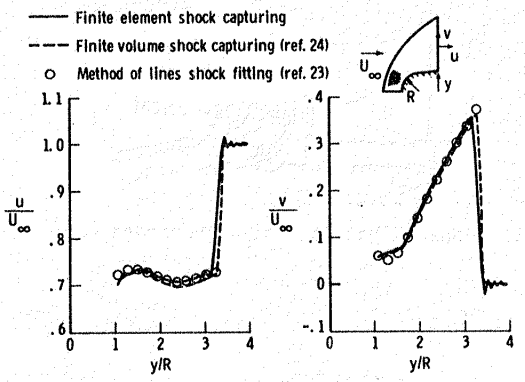

Fig. 12 Comparative solutions at outflow plane for flow over blunt leading edge of 8' HTT panel holder.

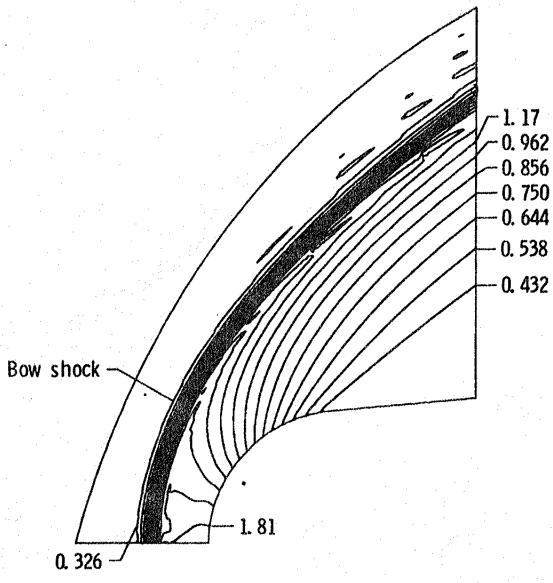

Fig. 11 Finite element predicted density contours for flow over blunt leading edge of 8' HTT panel holder (units are $x10^{-6}$ lb_m/in^3).

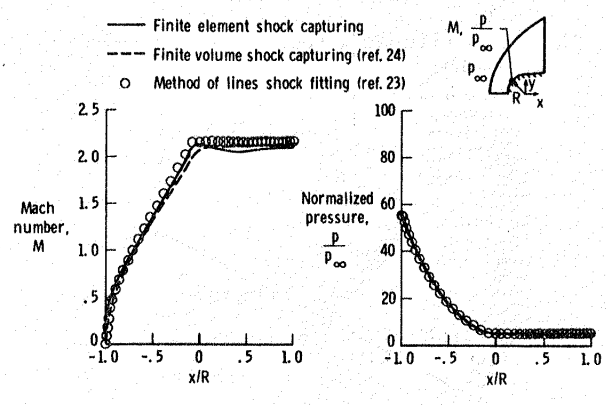

Fig. 13 Comparative solutions along the body surface for flow over blunt leading edge of 8' HTT panel holder.

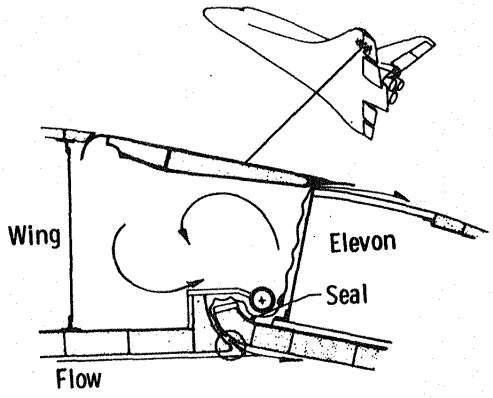

Fig. 14 Space Shuttle wing-elevon cove configuration.

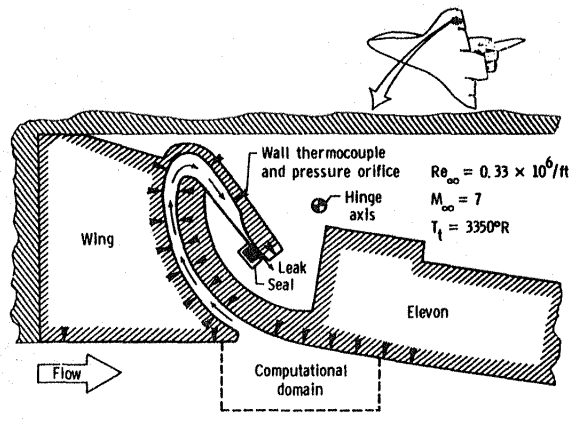

Fig. 15 Partial cross-section of experimental cove model.

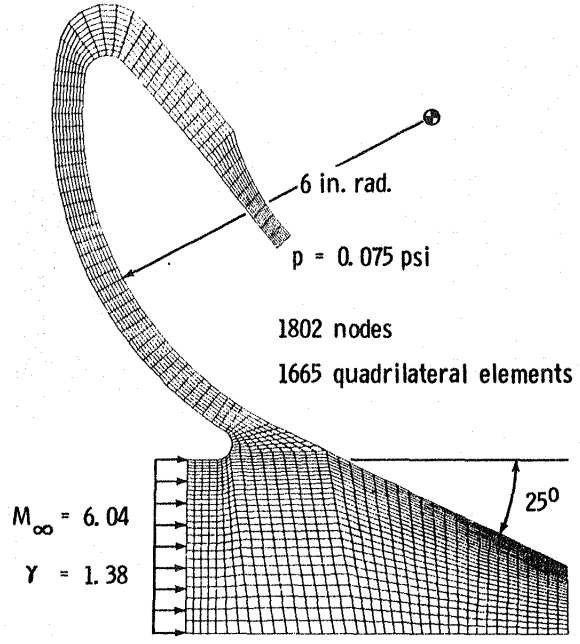

Fig. 16 Finite element mesh for flow in wing-elevon cove.

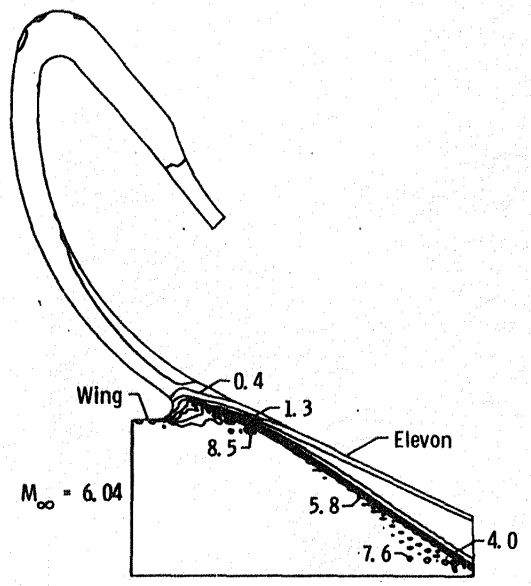

Fig. 17 Mach number contours for flow in wing-elevon cove.

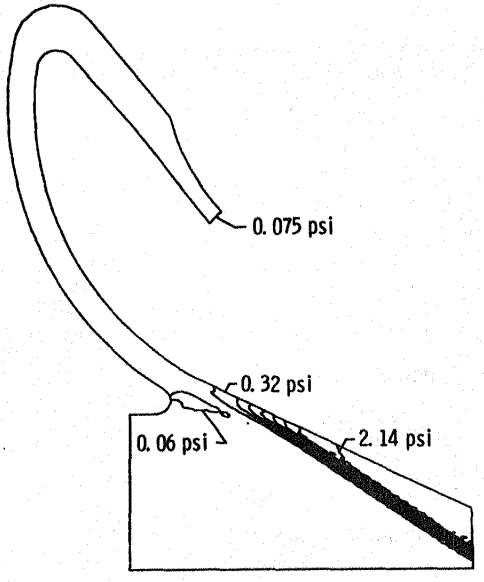

Fig. 18 Pressure contours for flow in wing-elevon cove.

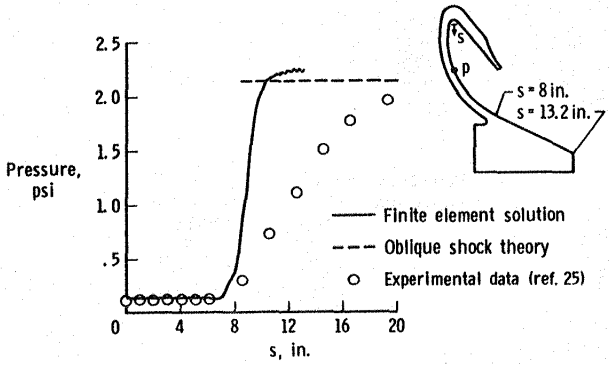

Fig. 19 Comparison of finite element predicted pressures and experimental data for wing-elevon cove.

1. Report No.	2. Government Accession No.	3. Recipient's Catalog No.
NASA TM-86434		

4. Title and Subtitle	5. Report Date
A New Finite Element Approach - Progress in Inviscid Flow Computations	July 1985
	6. Performing Organization Code: 506-53-33-04

7. Author(s)	8. Performing Organization Report No.
Kim S. Bey, Earl A. Thornton, Pramote Dechaumphai, and R. Ramakrishnan	
	10. Work Unit No.

9. Performing Organization Name and Address	11. Contract or Grant No.
Langley Research Center Hampton, VA 23665	
	13. Type of Report and Period Covered: Technical Memorandum

12. Sponsoring Agency Name and Address	14. Sponsoring Agency Code
National Aeronautics and Space Administration Washington, DC 20546	

15. Supplementary Notes: Kim S. Bey, NASA Langley Research Center, Hampton, Virginia. E. A. Thornton, P. Dechaumphai, and R. Ramakrishnan, Old Dominion Univ., Norfolk, VA. This paper is to be presented at AIAA 7th Computational Fluid Dynamics Conference, Cincinnati, OH, July 15-17, 1985. (AIAA Paper No. 85-1533-CP)

16. Abstract

Recent progress in the development of finite element methodology for the prediction of aerothermal loads is described. Two dimensional, inviscid computations are presented, but emphasis is placed on development of an approach extendable to three dimensional viscous flows. Research progress is described for: (1) utilization of a commerically available program to construct flow solution domains and display computational results, (2) development of an explicit Taylor-Galerkin solution algorithm, (3) closed form evaluation of finite element matrices, (4) vector computer programming strategies, and (5) validation of solutions. Two test problems of interest to NASA Langley aerothermal research are studied. Comparisons of finite element solutions for Mach 6 flow with other solution methods and experimental data validate fundamental capabilities of the approach for analyzing high speed inviscid compressible flows.

17. Key Words (Suggested by Author(s))	18. Distribution Statement
Finite Element High Speed Inviscid Flow	Unclassified-Unlimited Subject Category 34

19. Security Classif. (of this report)	20. Security Classif. (of this page)	21. No. of Pages	22. Price
Unclassified	Unclassified	15	A02

End of Document